Effect of self-propulsion on equilibrium clustering

Ethayaraja Mani[1,*] and Hartmut Löwen[2]

[1]*Polymer Engineering and Colloid Science Laboratory, Department of Chemical Engineering, Indian Institute of Technology Madras, Chennai 600036, India*

[2]*Institut für Theoretische Physik II: Weiche Materie, Heinrich-Heine-Universität Düsseldorf, Universitätsstraße 1, D-40225 Düsseldorf, Germany*

(Received 1 November 2014; revised manuscript received 27 June 2015; published 2 September 2015)

In equilibrium, colloidal suspensions governed by short-range attractive and long-range repulsive interactions form thermodynamically stable clusters. Using Brownian dynamics computer simulations, we investigate how this equilibrium clustering is affected when such particles are self-propelled. We find that the clustering process is stable under self-propulsion. For the range of interaction parameters studied and at low particle density, the cluster size increases with the speed of self-propulsion (activity) and for higher activity the cluster size decreases, showing a nonmonotonic variation of cluster size with activity. This clustering behavior is distinct from the pure kinetic (or motility-induced) clustering of self-propelling particles which is observed at significantly higher activities and densities. We present an equilibrium model incorporating the effect of activity as activity-induced attraction and repulsion by imposing that the strength of these interactions depend on activity superlinearly. The model explains the cluster size dependence of activity obtained from simulations semiquantitatively. Our predictions are verifiable in experiments on interacting synthetic colloidal microswimmers.

DOI: 10.1103/PhysRevE.92.032301 PACS number(s): 82.70.Dd, 64.75.Xc

I. INTRODUCTION

Concentrated colloidal or protein solutions which are governed by a combination of short-range attractive and long-range repulsive interaction potentials exhibit a stable clustering phenomenon in equilibrium at finite temperature and moderate densities. This phenomenon is first predicted by theory [1] and simulation [2–5] and has been confirmed in experiments [6,7]. The intuitive explanation [1] for equilibrium clustering lies in the fact that the short-ranged attraction first leads to growth of clusters in an initially dilute suspension of particles. The growth stops, however, when the cluster size reaches a characteristic size where the long-ranged repulsion leads to an increase in the self-energy of the cluster. In equilibrium, at finite temperature, this leads to a typical average cluster size which depends on the interaction parameters and the imposed global particle density. While the details of this equilibrium cluster process have been understood for a decade now, recent developments have considered self-propelled (or active) particles which dissipate energy, leading to synthetic microswimmers [8,9]. These particles also exhibit a purely kinetic clustering if the strength of self-propulsion is sufficiently large [9,10], which has recently been found in experiments [11–13] and explored by simulation [12,14–22] and theory [17,20,23–28]. This purely motility-induced clustering occurs for repulsive systems and is therefore absent in equilibrium (i.e., for vanishing drive). The study of Redner *et al.* [29] showed reentrant phase behavior in active Lennard-Jones particles, where attractive interaction and activity compete to stabilize phase-separated states at low and high activities, respectively.

Here we link the fields of equilibrium clustering to that of microswimmers. We consider the equilibrium clustering and study how this is affected by an imposed self-propulsion. The motivation to do so is threefold. First of all, this is an interesting problem in itself, since upon increasing the self-propulsion, there are two counterbalancing effects: on the one hand, the self-propulsion leads to a higher mobility and hence an effect which is expected to correspond to an increase of temperature. On the other hand, however, the self-propulsion yields a larger sticking probability of neighboring particles which would favor and enhance the clustering tendency. The second motivation comes from the fact that one needs to understand whether there is a hidden pathway between the two different kinds of clustering mentioned above, i.e., to check whether they are distinct or interconnected in a certain parameter space. Finally, artificial colloidal model microswimmers can be prepared with controlled interactions, e.g., by adding depletants [30], tuned van der Waals attractions, or charging the particles such that model colloidal swimmers can be prepared, in principle, with short-ranged attraction and long-ranged repulsion. The additional tunability of the interparticle potential then allows one to control the degree of clustering, which requires a systematic understanding.

In this paper we simulate a two-dimensional model of microswimmers with competing interactions by using Brownian dynamics computer simulations. We use a model proposed by Sear *et al.* [31] and Imperio and Reatto [3], for which the equilibrium clustering behavior is well understood in two dimensions, but supplement this here for an additional self-propulsion in the simplest form by neglecting explicit alignment and hydrodynamic interactions [32]. As a result, we find, indeed, that the trends of clustering depend on the interaction parameters. The self-propulsion can either increase or decrease the cluster size. In fact, there is a complex and maybe unanticipated nonmonotonic behavior of the cluster size as a function of increasing self-propulsion: it can first increase and then decrease again. This cannot be understood by simple temperature rescaling, as has been previously noted for active systems in the context of freezing [32] as well as in a trapping [33] and in a gravitational field [11]. Dynamic (or purely motility-induced) clustering also occurs in our

*ethaya@iitm.ac.in

model, although at much larger drives, where the details of the interactions become irrelevant. In this case, the cluster sizes are rather small compared to those of equilibrium clusters. Thus the two clustering phenomena appear quite distinct.

II. MODEL AND SIMULATION

We model short-range attractive and long-range repulsive interactions using a modified Lennard-Jones potential $u_1(r)$ and a double-exponential potential $u_2(r)$ that was introduced previously to explain the formation of finite-sized clusters and stripes of nanoparticles at the air-water interface [31]. The overall potential is given as

$$u(r) = u_1(r) + u_2(r). \tag{1}$$

Here $u_1(r)$ is defined as

$$u_1(r) = 4\epsilon_{LJ}\left[\left(\frac{\sigma_{LJ}}{r}\right)^{100} - \left(\frac{\sigma_{LJ}}{r}\right)^{50}\right] \tag{2}$$

and $u_2(r)$ is given by

$$u_2(r) = -\frac{\epsilon_a\sigma^2}{R_a^2}\exp\left(-\frac{r}{R_a}\right) + \frac{\epsilon_r\sigma^2}{R_r^2}\exp\left(-\frac{r}{R_r}\right). \tag{3}$$

Here r is the interparticle distance, and σ is the diameter of the particle. ϵ_{LJ} and σ_{LJ} are the parameters of the modified Lennard-Jones potential. We fix the potential parameters to $\sigma_{LJ} = \sigma$, $R_a = \sigma$, $R_r = 2\sigma$, and $\epsilon_a = \epsilon_r$. In the following, we use dimensionless quantities and express energy in units of k_BT, length in units of σ, and time in units of $\tau = \sigma^2/D$. Here, k_B is the Boltzmann constant, T is temperature, and D is the diffusion coefficient of a single passive particle. We further fix $\epsilon_{LJ} = 0.002\,5k_BT$. Figure 1 shows the variation of potential with interparticle distance for $\epsilon_a = 25k_BT$. Note that the repulsive part of the double-exponential potential is rather long ranged.

Brownian dynamics simulations in two dimensions in the xy plane are performed with particles interacting via the potential given in Eq. (1). We simulate $N = 1050$ particles using a square box with periodic boundary conditions. To mimic self-propulsion, the particles are defined with an orientation $\mathbf{e}_i$ diffusing freely about the perpendicular z axis with rotational diffusivity D_r. In two dimensions, the components of $\mathbf{e}_i$ are given as $\mathbf{e}_i = (\cos\varphi_i, \sin\varphi_i)$. In addition to translational Brownian motion, the particles are driven with constant speed v along their orientation $\mathbf{e}_i$. Here there are no aligning interactions, as the pair potential is independent of orientations. Moreover, hydrodynamics interactions are neglected. The resulting equations of motion for the particle positions $\{\mathbf{r}_i\}$ and orientations $\{\mathbf{e}_i\}$ are then given by

$$\dot{\mathbf{r}}_i = \frac{D}{k_BT}(-\nabla_{\mathbf{r}_i}U) + \mathbf{e}_i v + \boldsymbol{\xi}_i, \tag{4}$$

$$\dot{\varphi}_i = \xi_i^r. \tag{5}$$

Here, $U = \sum_{i<j} u(|\mathbf{r}_i - \mathbf{r}_j|)$ is the total pair potential. The self-propulsion speed of the particle is referred to in terms of the dimensionless Péclet number Pe defined as

$$\mathrm{Pe} = \frac{\sigma v}{D}. \tag{6}$$

The Gaussian noise $\boldsymbol{\xi}_i$ models the stochastic solvent kicks. It has a zero mean and variance $\langle\boldsymbol{\xi}_i(t)\boldsymbol{\xi}_j^T(t')\rangle = 2\delta_{ij}D\mathbf{1}\delta(t-t')$, where $\mathbf{1}$ is the identity matrix. Similarly, the stochastic random torque ξ_i^r has a zero mean and a variance of $\langle\xi_i^r(t)\xi_j^r(t')\rangle = 2D_r\delta_{ij}\delta(t-t')$. The rotational diffusivity is taken as $D_r = 3D/\sigma^2$, which is a valid approximation for a spherical particle undergoing free rotational diffusion. The equations of motion, Eqs. (4) and (5), are numerically integrated with a time step of $10^{-5}\tau$. The long-range potential Eq. (1) is truncated at $r = 15\sigma$. Simulations were done for various reduced areal densities (typically of $0.13\sigma^{-2}$ unless stated otherwise) and for different values of ϵ_a. The simulations are performed starting from a random initial configuration of particles. Typically the system is simulated for 500τ (i.e., 5×10^7 steps) to attain a steady state, followed by production runs of another 500τ. The simulations are replicated five times with different initial random configurations and the properties are time-averaged over all the replicas. Careful tests were performed to check that the system achieved a steady state by monitoring the saturation of the cluster size as a function of time and by making sure that there is enough exchange dynamics between the clusters.

To define a cluster we use a cutoff distance of 1.5σ, which corresponds to the interparticle distance where the potential is roughly half of the potential at contact. Two particles belong to the same cluster if they are connected by a sequence of other particles which are all separated by less than 1.5σ. The average cluster size is calculated from

$$\langle n\rangle = \sum_{n=1}^{N} nP(n). \tag{7}$$

Here, $P(n)$ is the probability to find a cluster of n number of particles at steady state. We also monitor the fluctuations in the cluster size by calculating the reduced variance

$$\mathrm{Var}(n) = \frac{\langle n^2\rangle - \langle n\rangle^2}{\langle n\rangle^2}. \tag{8}$$

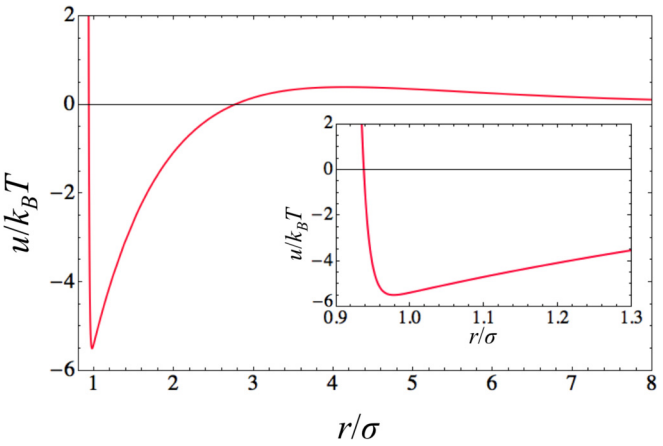

FIG. 1. (Color online) Overall interaction potential $u(r)$ showing competing attractive and repulsive interactions for $\epsilon_a = 25k_BT$ from Eq. (1). The inset shows the potential near contact.

III. CLUSTERING OF ACTIVE PARTICLES

Passive particles with short-ranged attractive and long-ranged repulsive interactions defined in Eq. (1) show

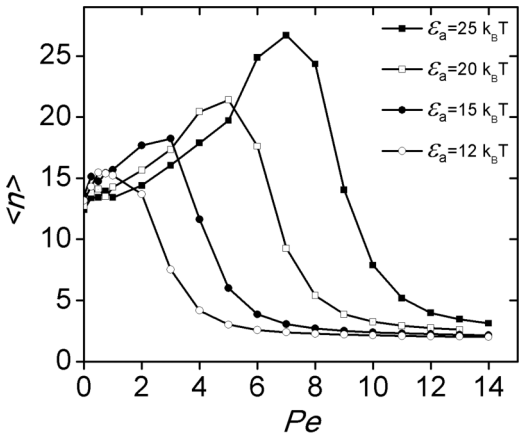

FIG. 2. Effect of activity on the average cluster size $\langle n \rangle$ for various values of ϵ_a. The lines serve as a guide to the eye.

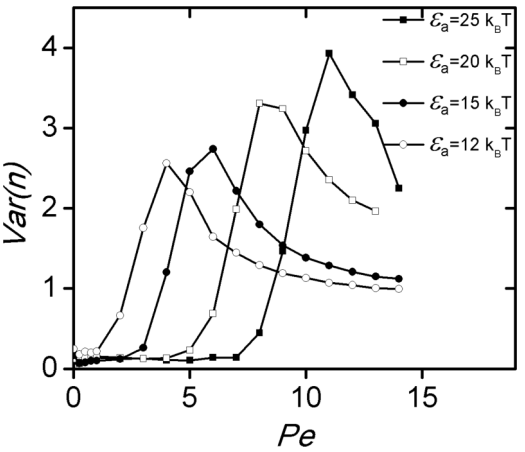

FIG. 4. Effect of activity on the reduced variance of cluster size for various ϵ_a values. The lines serve as a guide to the eye.

equilibrium clustering at certain densities. In particular, equilibrium clustering occurs for a density of about 0.13 and for attraction energies ϵ_a in the range of $12k_BT$ to $25k_BT$ [3]. These clusters are quasicircular in shape. The effect of activity on clustering is shown in Fig. 2, where the average cluster size $\langle n \rangle$ is shown versus the Péclet number Pe. For the cases of vanishing activity, the average cluster size is about $\langle n \rangle \approx 14$ independent of ϵ_a.

Strikingly, the dependence of the average cluster size on activity is nonmonotonic. The cluster size first increases with increasing activity and attains a maximum before it finally decreases at higher activity. This trend is seen for all the ϵ_a values studied here. The critical activity corresponding to the maximum of cluster size increases with increasing ϵ_a. This behavior points to the possibility that the activity manifests itself as an effective attraction which increases the cluster size until the activity gets so high that particles are eventually removed from the cluster, overcoming attractive interactions between the particles in the cluster. It is interesting that we find a maximum in the cluster size at intermediate Pe, while Redner *et al.* [29] find a suppression of phase separation at intermediate Pe. Therefore our findings are qualitatively different from those of Redner *et al.* [29] due to the combination of attraction and repulsion.

Representative snapshots showing clusters for Pe = 0 and Pe = 6 (at fixed $\epsilon_a = 25k_BT$) are shown in Figs. 3(a) and 3(b), respectively. The clusters exhibit an inner crystalline structure as found in previous simulations for dynamical clustering [12]. Moreover, there is a large spread in cluster sizes. This is also documented by the normalized size distribution function $P(n)$, which is shown in the insets of Figs. 3(a) and 3(b). An increased activity leads to a much larger distribution in the cluster size at steady state. This is documented by the reduced variance of the cluster size distribution, which steeply increases with Pe as shown in Fig. 4 until it reaches a maximum and decreases as it is correlated with the average cluster size.

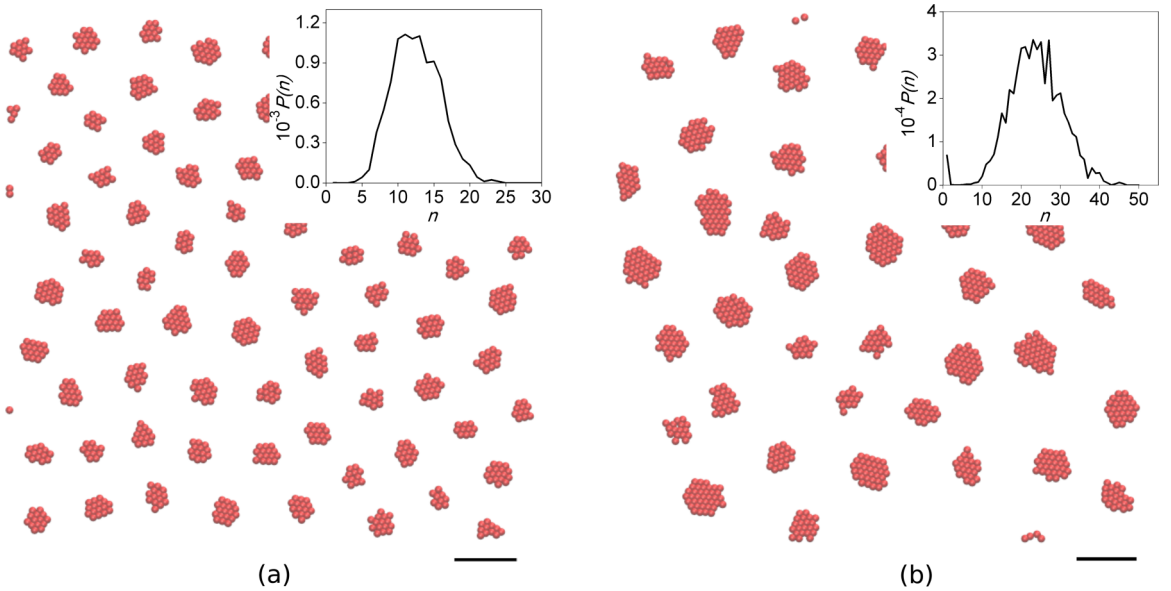

FIG. 3. (Color online) Representative snapshots of clusters for Pe = 0 (a) and Pe = 6 (b) for $\epsilon_a = 25k_BT$. The insets show the cluster size distribution $P(n)$ in the steady state. The scale bars correspond to 10σ.

IV. EFFECTIVE EQUILIBRIUM MODEL

We now present a phenomenological model to explain the clustering behavior observed in active particles by balancing interparticle interactions with activity. First we consider passive particles with short-ranged attractive and long-ranged repulsive interactions and include the effect of activity in the model later. Consider monomeric disks of diameter σ assembled as circular clusters of uniform diameter d with n number of monomers. The disks interact with themselves via a short-range attraction and long-range repulsion. Following the approach of Groenewold and Kegel [1], the free energy of such a cluster of passive particles can be written as

$$f(n) = \frac{gn^2 E_r \sigma}{d} - nE_a + \pi d\lambda, \tag{9}$$

where g is a geometric parameter related to circular shape, and E_r and E_a are typical repulsive and attractive energies of a particle inside the cluster. The first term accounts for total repulsive energy and is of order n^2 due to the long-range nature of repulsion; the second term accounts for attractive energy assuming the attraction to be short ranged and therefore scales linear in n. The last term is energy due to line tension λ of the cluster boundary. Also note that n and d are related via

$$n = \frac{\pi d^2}{4a}, \tag{10}$$

where a is the cross-sectional area of the monomer ($a = \pi\sigma^2/4$). Combining Eqs. (9) and (10) we get

$$\frac{f(n)}{n} = \sqrt{\frac{\pi}{a}} g E_r \sqrt{n} - E_a + 2\lambda\sqrt{\pi a}\frac{1}{\sqrt{n}}. \tag{11}$$

Minimizing Eq. (11) with respect to n yields an equilibrium cluster size n^*:

$$n^* = \frac{2a\lambda}{gE_r}. \tag{12}$$

Approximating the line tension as $\lambda \approx E_a/\sigma$, the equilibrium cluster size is given as

$$n^* = \frac{\pi\sigma E_a}{2gE_r}. \tag{13}$$

Equation (13) gives the effect of interaction parameters on the equilibrium cluster size of passive particles with short-ranged attractive and long-ranged repulsive interactions. We use Eq. (13) as a starting point to analyze active particles, wherein each particle propels with a speed of v and rotates freely in two dimensions in addition to their short-ranged attractive and long-ranged repulsive interparticle interactions. The critical issue is to know how to incorporate the effect of activity in terms of *effective* attractive and repulsive interactions in Eq. (13). Consistent with previous work [11,30,34], we propose that the role of activity in affecting interparticle interactions has the following features:

(1) Both effective attraction and repulsion increase with Pe.

(2) For small Pe, the increase of an activity-induced effective attraction is more pronounced than the activity-induced effective repulsion.

TABLE I. Fit parameters used in the effective equilibrium model.

$\epsilon_a(k_BT)$	$E_a(k_BT)$	$E_r(k_BT)$	a	b
12	2.6	0.18	1.0605	0.0142
15	3.3	0.21	0.5928	0.0030
20	4.4	0.31	0.4550	0.0008
25	5.5	0.38	0.3226	0.0002

(3) For large Pe, the effective activity-induced repulsion is getting more pronounced than the activity-induced effective attraction.

Therefore we replace E_a in Eq. (13) to account for an effective activity-induced attraction as $E_a + a\mathrm{Pe}^p$ with two fit parameters: an amplitude a and an exponent p. Similarly, we add to E_r an activity-induced repulsion, i.e., we replace E_r by $E_r + b\mathrm{Pe}^q$ with two fit parameters, namely, an amplitude b and an exponent q which is larger than p. Therefore

$$n^* = \frac{\pi\sigma(E_a + a\mathrm{Pe}^p)}{2g(E_r + b\mathrm{Pe}^q)} \tag{14}$$

We find reasonable fits for our simulation data when fixing $p = 2$ and $q = 4$ by adjusting only the amplitudes a and b. The actual fit parameters are given in Table I, and in Fig. 5 the comparison between the model and simulation data is shown. Good fits are obtained for small ϵ_a, but deviations are visible for larger ϵ_a. Here, the values of E_a and E_r correspond to the minimum and maximum of the potential described in Eq. (1). The parameter $g = 1.83$ is chosen such that the model predicts the size of the cluster size in the absence of activity. Hence this phenomenological model can give account for the trends that at low Pe, $\langle n\rangle$ increases and then decreases for high Pe.

V. EQUILIBRIUM VERSUS DYNAMICAL CLUSTERING

Next we discuss the state behavior of active particles with competing interactions to understand the link between equilibrium clustering and kinetic clustering induced by activity. Representative configurations obtained from simulations for different density and activity are shown in Fig. 6 and a

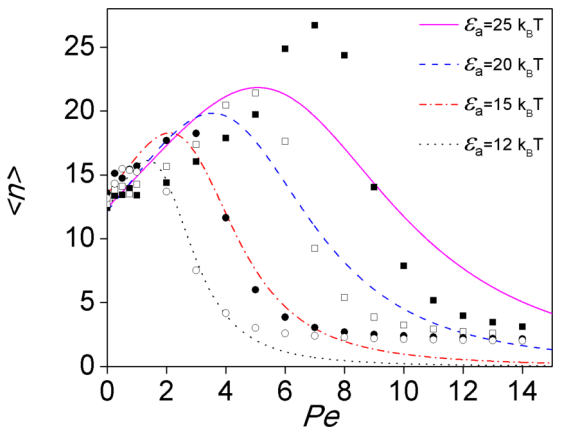

FIG. 5. (Color online) Comparison between predictions of the model [Eq. (14)] (lines) with simulation data (points). Legends for the data points are same as in Fig. 2.

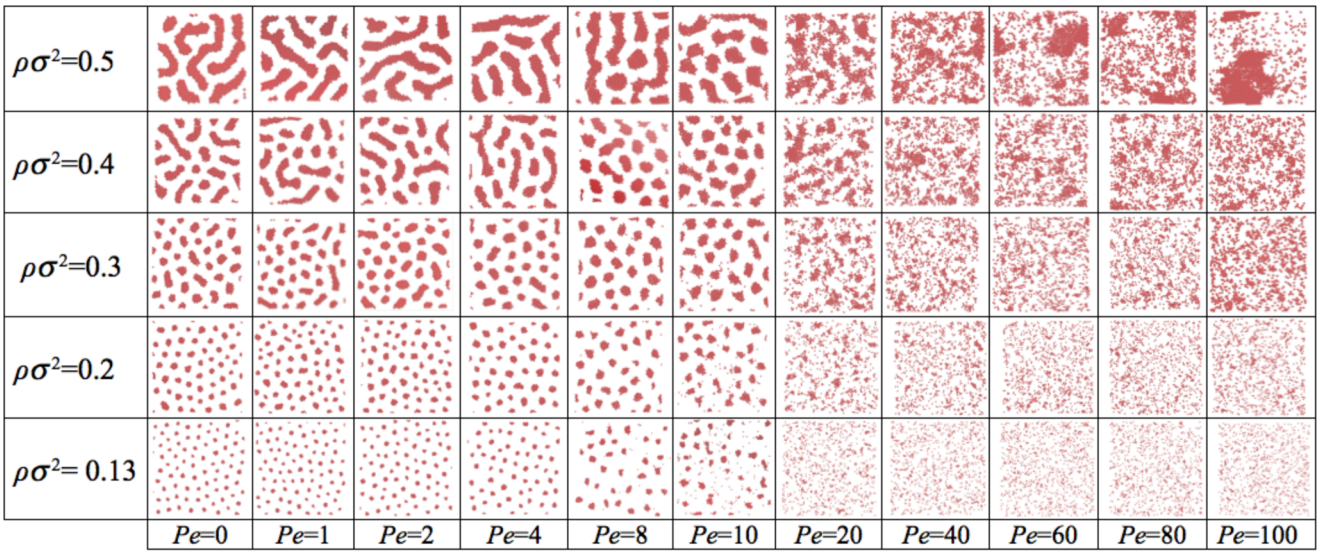

FIG. 6. (Color online) Representative configurations of various states of active particles with competing interactions for varied Péclet number Pe and reduced number density $\rho\sigma^2$ for $\epsilon_a = 25k_BT$.

corresponding state diagram is presented in Fig. 7. In the absence of activity (Pe = 0), the particles form quasicircular clusters at low density and extended wormlike clusters at higher densities. Upon increasing activity the phase behavior changes significantly. For instance, up to a reduced density of 0.2, the activity increases the cluster sizes until a critical activity is reached and beyond this activity clusters dissolve, leading to a disordered fluid phase. In the density range of 0.3–0.4, we see a similar behavior but now the elongated wormlike clusters are getting smaller in length upon increasing the activity. Further increase in activity again leads to a disordered fluid in this density regime. At higher densities such as 0.5, the disordered fluid is followed by phase separation due to kinetic clustering induced by motility, as found in earlier reports on purely repulsive particles [12,17]. At these high Péclet numbers, details of the interparticle interaction except for the repulsive core are not relevant. The dynamic clustering observed at high Pe is therefore explained as a pure kinetic effect. It is well separated from the equilibrium clustering considered earlier which occurs at small Pe and small densities, demonstrating that these two clustering effects are qualitatively distinct.

We now revisit the cluster size distribution function $P(n)$ in the limit of high Péclet numbers where only the repulsive core is relevant, which is then to be compared to the previous data shown in Fig. 3. Results for Pe = 100 are shown in Fig. 8 on a semilog scale. The average cluster size in this case is 1.8. The clusters are distinctly different, both in size and shape, from that observed in equilibrium [Fig. 3(a)] and at moderate activity [Fig. 3(b)], although ϵ_a and density are the same. This means that activity can be used as a knob, to an extent, in tuning the cluster size either to increase or to decrease, depending upon the fixed parameters of interactions. This unique feature is not present for purely motility-induced clustering in repulsive colloids. In more detail, as can be deduced from Fig. 8, the cluster size distribution $P(n)$ is almost linear in the semilogarithmic plot, except for small n ($n < 4$). This shows that there is an exponential decay in $P(n)$ for large n. The data for $n < 5$ are compatible with a power-law scaling. Majumdar *et al.* [35] showed that for an effective aggregating

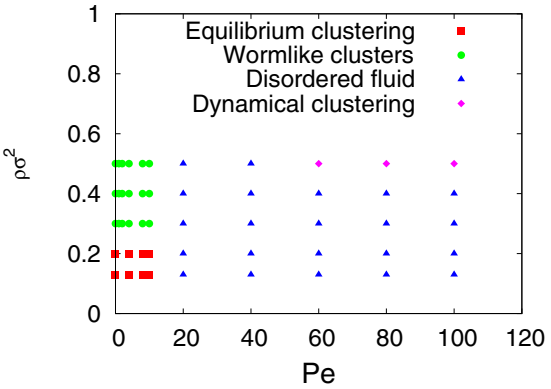

FIG. 7. (Color online) State diagram of active particles with competing interactions in the plane spanned by Péclet number Pe and reduced density $\rho\sigma^2$ for $\epsilon_a = 25k_BT$.

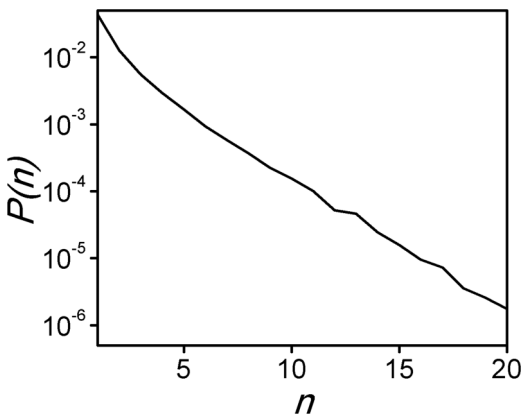

FIG. 8. Cluster size distribution for Pe = 100, density $\rho\sigma^2 = 0.13$, and $\epsilon_a = 25k_BT$.

and fragmenting particle system, $P(n)$ decays exponentially for low aggregation rates and decays as power law for high aggregation rates. In the present case, the initial power-law decay denoting an effective aggregation process indicates motility-induced kinetic clustering at high Péclet numbers. The exponential decay denoting effective fragmentation indicates fragmentation due to activity. Therefore, high activity induces both aggregating and fragmenting processes. In contrast, in the case of $\mathrm{Pe} = 6$, where both the interaction potential and activity affect clustering, the cluster size distribution $P(n)$ does not show any conclusive scaling.

Furthermore, we note that our results are different from flying crystals which were found to exist with and without cohesive forces [36–38]. In these studies, aligning forces between the particles are relevant. In our simulations, we have not considered aligning forces and therefore we have not observed flying crystals. The velocity vectors of the particles in the clusters obtained from our simulations are randomly oriented as the particles are freely rotating with their rotational diffusion coefficient. Therefore there is only a random and undirected migration of the clusters.

VI. CONCLUSION

In conclusion, by using Brownian dynamics computer simulations, we explored how equilibrium clustering is affected for self-propelled colloidal particles. While this clustering process is stable under self-propulsion, depending on the values of interaction parameter, the cluster size can initially increase with the strength of self-propulsion before it decreases for large activity. This allows one to control the strength of active clustering via the interparticle interactions. A phenomenological model is shown to qualitatively explain the nonmonotonic variation of cluster size with activity. For the future, it would be interesting to construct a dynamical density functional theory for the clustering considered here by unifying the density functional theory designed for equilibrium clustering [39] with that designed for kinetic clustering [17]. Moreover, hydrodynamic effects should be explored by more sophisticated simulation models [40]. Furthermore, our predictions can in principle be verified in experiments on synthetic or bacterial microswimmers with well-defined interactions. In particular, the combination of depletants, particle charge, and magnetic dipole moments [41,42] opens new ways to steer the interparticle interactions between swimmers and therefore the details of the clustering behavior.

ACKNOWLEDGMENTS

We thank Julian Bialké, Andreas Kaiser, and Borge ten Hagen for helpful discussions. E.M. acknowledges DAAD for Research Stay fellowship and H.L. acknowledges support from the European Research Council under the European Union's Seventh Framework Programme, Grant Agreement No. 267499.

[1] J. Groenewold and W. K. Kegel, J. Phys. Chem. B **105**, 11702 (2001).
[2] F. Sciortino, S. Mossa, E. Zaccarelli, and P. Tartaglia, Phys. Rev. Lett. **93**, 055701 (2004).
[3] A. Imperio and L. Reatto, J. Chem. Phys. **124**, 164712 (2006).
[4] P. D. Godfrin, R. Castañeda-Priego, Y. Liu, and N. J. Wagner, J. Chem. Phys. **139**, 154904 (2013).
[5] E. Mani, W. Lechner, W. K. Kegel, and P. G. Bolhuis, Soft Matter **10**, 4479 (2014).
[6] A. Stradner, H. Sedgwick, F. Cardinaux, W. C. K. Poon, S. U. Egelhaaf, and P. Schurtenberger, Nature (London) **432**, 492 (2004).
[7] A. I. Campbell, V. J. Anderson, J. S. van Duijneveldt, and P. Bartlett, Phys. Rev. Lett. **94**, 208301 (2005).
[8] P. Romanczuk, U. Erdmann, H. Engel, and L. Schimansky-Geier, Eur. Phys. J.: Spec. Top. **157**, 61 (2008).
[9] M. Marchetti, J. Joanny, S. Ramaswamy, T. Liverpool, J. Prost, M. Rao, and R. Simha, Rev. Mod. Phys. **85**, 1143 (2013).
[10] J. Bialké, T. Speck, and H. Löwen, J. Non-Cryst. Solids **407**, 367 (2015).
[11] F. Ginot, I. Theurkauff, D. Levis, C. Ybert, L. Bocquet, L. Berthier, and C. Cottin-Bizonne, Phys. Rev. X **5**, 011004 (2015).
[12] I. Buttinoni, J. Bialké, F. Kümmel, H. Löwen, C. Bechinger, and T. Speck, Phys. Rev. Lett. **110**, 238301 (2013).
[13] J. Palacci, S. Sacanna, A. Steinberg, D. Pine, and P. Chaikin, Science **339**, 936 (2013).
[14] Y. Fily and M. C. Marchetti, Phys. Rev. Lett. **108**, 235702 (2012).
[15] J. Stenhammar, A. Tiribocchi, R. J. Allen, D. Marenduzzo, and M. E. Cates, Phys. Rev. Lett. **111**, 145702 (2013).
[16] G. S. Redner, M. F. Hagan, and A. Baskaran, Phys. Rev. Lett. **110**, 055701 (2013).
[17] J. Bialké, H. Löwen, and T. Speck, Europhys. Lett. **103**, 30008 (2013).
[18] J. Stenhammar, D. Marenduzzo, R. J. Allen, and M. E. Cates, Soft Matter **10**, 1489 (2014).
[19] Y. Fily, S. Henkes, and M. C. Marchetti, Soft Matter **10**, 2132 (2014).
[20] T. Speck, J. Bialké, A. M. Menzel, and H. Löwen, Phys. Rev. Lett. **112**, 218304 (2014).
[21] A. Wysocki, R. G. Winkler, and G. Gompper, Europhys. Lett. **105**, 48004 (2014).
[22] B. M. Mognetti, A. Šarić, S. Angioletti-Uberti, A. Cacciuto, C. Valeriani, and D. Frenkel, Phys. Rev. Lett. **111**, 245702 (2013).
[23] J. Tailleur and M. E. Cates, Phys. Rev. Lett. **100**, 218103 (2008).
[24] M. E. Cates, D. Marenduzzo, I. Pagonabarraga, and J. Tailleur, Proc. Natl. Acad. Sci. USA **107**, 11715 (2010).
[25] M. E. Cates and J. Tailleur, Europhys. Lett. **101**, 20010 (2013).
[26] R. Wittkowski, A. Tiribocchi, J. Stenhammar, R. J. Allen, D. Marenduzzo, and M. E. Cates, Nat. Commun. **5**, 4351 (2014).
[27] F. Peruani and M. Bär, New J. Phys. **15**, 065009 (2013).
[28] P. Cremer and H. Löwen, Phys. Rev. E **89**, 022307 (2014).
[29] G. S. Redner, A. Baskaran, and M. F. Hagan, Phys. Rev. E **88**, 012305 (2013).
[30] J. Schwarz-Linek, C. Valeriani, A. Cacciuto, M. E. Cates, D. Marenduzzo, A. N. Morozov, and W. C. K. Poon, Proc. Natl. Acad. Sci. USA **109**, 4052 (2012).
[31] R. P. Sear, S.-W. Chung, G. Markovich, W. M. Gelbart, and J. R. Heath, Phys. Rev. E **59**, R6255 (1999).

[32] J. Bialké, T. Speck, and H. Löwen, Phys. Rev. Lett. **108**, 168301 (2012).
[33] G. Szamel, Phys. Rev. E **90**, 012111 (2014).
[34] T. F. F. Farage, P. Krinninger, and J. M. Brader, Phys. Rev. E **91**, 042310 (2015).
[35] S. N. Majumdar, S. Krishnamurthy, and M. Barma, Phys. Rev. Lett. **81**, 3691 (1998).
[36] G. Gregoire and H. Chaté, Phys. Rev. Lett. **92**, 025702 (2004).
[37] J. Toner, Y. Tu, and S. Ramaswamy, Ann. Phys. **318**, 170 (2005).
[38] A. M. Menzel and H. Löwen, Phys. Rev. Lett. **110**, 055702 (2013).
[39] T. Jiang and J. Wu, Phys. Rev. E **80**, 021401 (2009).
[40] A. Zöttl and H. Stark, Phys. Rev. Lett. **112**, 118101 (2014).
[41] L. Baraban, D. Makarov, O. G. Schmidt, G. Cuniberti, P. Leiderer, and A. Erbe, Nanoscale **5**, 1332 (2013).
[42] L. Baraban, R. Streubel, D. Makarov, L. Han, D. Karnaushenko, O. G. Schmidt, and G. Cuniberti, ACS Nano **7**, 1360 (2013).